Analyst

CRITICAL REVIEW

View Article Online
View Journal | View Issue



Cite this: *Analyst*, 2017, **142**, 1654

# Charge detection mass spectrometry: weighing heavier things

David Z. Keifer,†[a] Elizabeth E. Pierson†[b] and Martin F. Jarrold *[c]

Received 16th February 2017,
Accepted 6th April 2017

DOI: 10.1039/c7an00277g

rsc.li/analyst

Charge detection mass spectrometry (CDMS) is a single molecule method where the mass of each ion is directly determined from individual measurements of its mass-to-charge ratio and charge. CDMS is particularly valuable for the analysis of high mass and heterogeneous analytes, where conventional MS methods are often confounded. In the last few years, CDMS has received a renaissance. Technical developments have improved the resolution and dramatically increased the breadth of problems that can be addressed. These improvements have moved CDMS more into the mainstream as interest in the application of mass spectrometry to high molecular weight species has grown. In the article, the three main variants of CDMS are described, along with an overview of recent applications.



## Introduction

Over the last several decades, a series of advances have allowed mass spectrometry (MS) to measure masses for larger and larger ions. While there is a risk of speaking prematurely, it seems that the upper limit of what can be achieved with conventional MS is being approached. By conventional MS we mean measuring the mass-to-charge ratios ($m/z$) of an ensemble of ions and then deducing the masses of those ions from peaks in the $m/z$ spectrum. This is the approach used in commercial instruments. Heck and coworkers have suggested that 20 MDa is the high-mass limit for conventional electrospray MS.[1] For species that are intrinsically heterogeneous the limit is considerably smaller.

Several factors contribute to the high-mass limit in conventional MS. First, common detectors such as microchannel plates have low detection efficiencies for high-$m/z$ ions.[2–4] Of the two ionization methods most frequently used for high-mass MS, MALDI (matrix-assisted laser desorption ionization) and electrospray, MALDI produces ions with lower charge and thus higher $m/z$, so detection efficiency is higher for the more highly charged ions from electrospray. However, the higher charge makes it more challenging to resolve charge state peaks in the $m/z$ spectrum. For very large ions, the necessary charge state resolution is often lacking. This is usually attributed to peak broadening from incomplete desolvation[5,6] or from intrinsic heterogeneity.[7–10] Large analytes like nanoparticles, cells, and aerosols are likely to be intrinsically heterogeneous. Field induced charge loss may also contribute to the poor charge state resolution for highly charged ions.[11] A final factor limiting the mass range results from the substantial kinetic energy that very large ions can acquire. Electrosprayed ions pick up this energy from the expansion into vacuum,[12] while ions generated by MALDI pick it up in the plume from the laser shot.[13] The ions need to be cooled as much as possible to improve ion transmission and focusing through the instrument. This is usually accomplished by increasing the background gas pressure in the first couple of regions of the instrument[12–14] and by using heavier background gases.[15] The pumping systems must therefore be capable of handling large gas loads. Increasing the background gas pressure has the added benefit of improving ion desolvation. Heating the inlet in electrospray mass spectrometers also improves desolvation.[16]

Despite the challenges outlined above, several groups have succeeded in doing conventional MS in the multi-MDa range. Robinson and coworkers were the first to succeed in this area, achieving barely resolved charge state peaks for the 2.5 MDa MS2 virus capsid with TOF-MS[17] (a capsid is the protein shell that surrounds the genetic material in a virus). Later, Heck and coworkers achieved well-resolved $m/z$ spectra of virus capsids formed from the assembly domain of Hepatitis B virus capsid protein.[10] These capsids exhibit two morphologies weighing around 3 and 4 MDa. The highest mass analyzed by conventional MS to date is the 18 MDa, Prohead I form of the HK97 virus capsid,[1] although there was only incipient resolution in the $m/z$ spectrum presumably due to incomplete desolvation. Conventional MS in the multi-MDa mass range usually requires homogeneous samples, or limited heterogeneity.[18] It

[a]*Department of Chemistry, Salisbury University, 1101 Camden Ave, Salisbury, MD 21801, USA*
[b]*Department of Analytical Sciences, Pharmaceutical Sciences and Clinical Supplies, Merck Research Laboratories, Merck & Co., Inc., Rahway, New Jersey 07065, USA*
[c]*Chemistry Department, Indiana University, 800 E. Kirkwood Ave, Bloomington, IN 47401, USA. E-mail: mfj@iu.edu*
†These authors contributed equally.

is no accident that all the examples mentioned above are for virus capsids which are usually composed of a specific number of identical proteins and are homogeneous in mass.

One way to overcome the limitations described above is to directly determine the mass of each ion. In addition to enabling mass measurements for much larger ions, this approach also provides an opportunity to investigate the properties of single ions. For example, fragmentation pathways of poly(ethylene oxide) polymers[19] and DNA molecules[20] have been discovered that would not be accessible from an ensemble measurement. A variety of single-molecule MS techniques have been developed over the last half-century or so.[21]

Several single-molecule MS methods determine mass by making a very accurate $m/z$ measurement for a single ion, shifting the charge, and then re-measuring the $m/z$. These methods include single-molecule FTICR (Fourier transform ion cyclotron resonance)[22,23] and quadrupole ion traps with optical detection.[24–26] They are the most accurate single-molecule MS methods, and since single ions can be trapped nearly indefinitely in these traps, their properties can be tracked over extended periods. In this vein, they have been used to investigate the photoluminescence of single quantum dots and the thermal stability of nanoparticles.[27] However, these techniques are not well-suited to determining mass distributions because mass measurements are time-consuming, often taking several minutes per ion.[25,26]

Nanomechanical oscillators provide another means to do a single-molecule mass measurement. Here, the resonant frequencies of a nano-scale oscillator are monitored. As single molecules accrete on the oscillator, changes in the resonant frequencies are used to determine mass.[28,29] The approach has been used to measure the masses of neutral molecules as well as ions.[30] However, mass measurements are not yet as accurate as many other single-molecule MS techniques.[21]

In the third class of single-molecule MS techniques the $m/z$ and the charge of single ions are measured and then multiplied to determine the mass. This has been done with FTICR,[31] where the charge of a single trapped ion is determined from the magnitude of the charge induced on the detector plates. However, the charge cannot be determined accurately using this approach because the induced charge also depends on the ion's trajectory in the trap. A quadrupole ion trap has also been used to measure the $m/z$ and charge of single ions. The $m/z$ was determined by ejecting the ion from the trap operated in the axial instability mode, and the charge was measured as the ejected ion strikes a charge-detecting plate.[32,33] The charge determination is inaccurate here as well. TOF (time of flight) MS with kinetic energy-dependent, cryogenic detectors is yet another technique in this class.[34] However, the detector response is not linearly proportional to the ion charge, so charge determination is difficult even for low charges.[35,36] Charge detection mass spectrometry (CDMS) is the final method in this class of single-molecule MS methods, and it is the focus of this review.

In CDMS an ion is passed through a metal tube. A positive ion entering an isolated conducting tube induces a negative charge on the inner surface and a positive charge on the outside. The induced charges are maintained until the ion exits, at which point they dissipate. As the length of the tube increases the magnitude of the induced charge approaches the charge on the ion.[37,38] Usually a length to diameter ratio of four or greater is used. With this aspect ratio, the induced charge is within a fraction of a percent of the measured charge for most locations of the ion within the cylinder. The fact that the induced charge is almost independent of the ions location in the cylinder is the key to measuring the charge accurately. This helps to clarify the difference between CDMS and single-ion FT-ICR (see above) where the magnitude of the induced charge depends on the ions trajectory and specifically how closely the ion approaches the detector plates. In single pass CDMS, the simplest kind; the $m/z$ is determined from the TOF through the tube (and the ion's kinetic energy). In linear array CDMS, multiple detector tubes are aligned. The charge is measured multiple times, reducing the root mean square (RMS) uncertainty in the charge by the square root of the number of measurements. To improve the charge measurement further, the detector tube can be embedded in an electrostatic ion trap, so a single ion's charge can be measured hundreds or thousands of times as the ion oscillates back and forth through the tube. This version is called ion trap CDMS. In this case, the $m/z$ is usually determined from the ion's oscillation frequency. Ion trap CDMS is the most accurate form of CDMS, but it is also the slowest. Single pass CDMS is the least accurate but fastest, while linear array CDMS is in the middle.[21] With recent innovations in ion trap CDMS, it is possible to measure the charge with essentially perfect accuracy.

The first part of this review focuses on how CDMS instrumentation has developed since its invention. This is followed by an overview of recent applications.

## Single-pass CDMS

The development of CDMS can be traced to the space race in the late 1950s, and specifically interest in the hypervelocity impact of micrometeorites on space craft and satellites. In 1960, Shelton and coworkers invented a method to measure the masses of charged, micron-sized iron particles before they were impacted on various surfaces to investigate the relationship between the impact crater and the particle size and velocity.[39] The particles were charged to around +10 000 elementary charges ($e$) by collision with a high voltage electrode, and then accelerated through a 100 kV potential to velocities of 1–3 km $s^{-1}$. Before striking the target surface, the high-energy particles were sent through two charge detector tubes in series. The signals from the tubes were amplified and displayed on an oscilloscope. The velocity, which provides the $m/z$, was determined from the time between the ion's entrance into the first tube and its exit from the second tube. The charge was determined from the size of the induced charge. Particle masses were determined to within about 20%. Friichtenicht subsequently used a Van de Graaff accelerator to accelerate

particles through larger potentials.[40] A further innovation was made shortly after by Rudolph.[41] In this work, each particle was flown through a detector tube for preliminary velocity and charge measurements. If these measurements did not fall within desired ranges, the particle was deflected away from the target. The measurement of up to 100 particles per second has been reported.[42] Recently, Continetti and coworkers have described a new apparatus to investigate nanoparticle surface impact phenomena.[43]

In 1995, Fuerstenau and Benner applied the induced charge approach to the study of electrosprayed nanoparticles and biological macromolecules in the 1–100 MDa mass range and coined the term "charge detection mass spectrometry" in the process.[44] This work was the springboard for subsequent CDMS studies because the mass range was more relevant to analytes of interest to chemists and biologists, and because electrospray was a viable ionization source for biological analytes. In single-pass CDMS, noise on the signal defines the uncertainty in the charge measurement. In the first experiments, the RMS uncertainty was about 150$e$ RMS, and the limit of detection (the smallest charge that could be reliably measured) was ~425$e$. Within a few years, the uncertainty had been reduced to ~50$e$.[45,46] The charges on electrosprayed ions are correlated with their mass, so ions as small as ~500 kDa were detectable.

The charge induced on the outside of the conducting tube by an approaching ion is detected by a charge sensitive preamplifier. The resulting signal (which is approximately trapezoidal) is often processed with a Gaussian shaping amplifier that yields a pulse when an ion enters the tube and a pulse of the opposite polarity when it exits. The ion charge is usually determined from the pulse amplitudes, in which case the shaping time constants must be much longer than the rise and fall times of the induced charge. The charge does not suddenly appear as the ion enters the detection tube; it starts to build-up as the ion approaches the tube and does not reach its full value until after the ion has gone a short distance into the tube. Thus the rise and fall times depend on the ion velocity and the diameter of the tube. If the rise and fall times are not much shorter than the shaping time constant, the pulse amplitudes depend on the ion velocity, and the charge must be determined from the pulse area. The charge measurement is usually calibrated by applying a test signal to the detector tube through a known capacitance. The number of ions passing through the detector tube per second must be kept small enough that the probability of having two ions in the detector tube at the same time is negligible.

In single-pass CDMS, the $m/z$ is determined from the flight time through the tube, which is obtained from the entrance and exit pulses of the ion. Because some of the charge is induced before the ion enters the tube, the apparent length of the tube can differ from its physical length.[45] Moreover, the flight time depends on the ion energy. The energy gained as the ions are accelerated through a known potential difference is easily determined, but ions also acquire energy from the expansion in the electrospray interface. The average excess energy can be determined by grounding the electrodes in the source region (so that the ions are not accelerated through a potential difference) and measuring the average ion velocity through the detector tube.[44,46–53] However, there is a distribution of ion energies from the gas expansion that this method does not account for,[54] and it causes tailing of the peaks.[44] Two methods have been used to correct for the excess energy. In the first, an ion is passed through a charge detector tube, and its velocity is measured from the TOF. The ion then enters a pulsed acceleration tube which is grounded while the ion enters and then pulsed to a high potential so that the ion is accelerated when it exits. The accelerated ion is then passed through a second detector tube. The difference in velocities along with the acceleration potential provides the $m/z$ of the ion.[55] In the second method, the ion's velocity is measured through the first detector tube as usual, and then it is accelerated and decelerated through a potential ramp before passing through a second detector tube. To deduce the $m/z$, the arrival time at the second tube is compared with what the arrival time would have been without the potential ramp.[56] Despite the complications caused by the excess energy, the $m/z$ measurement in single-pass CDMS is still about an order of magnitude more precise than the charge measurement.[44]

Because the charge uncertainty of single-pass CDMS is fundamentally limited by detector noise, modern single-pass CDMS is still imprecise, with charge uncertainties often no better than ~50$e$.[45] Also, since an ion can only be detected by its signal rising clearly above the noise, the limit of detection (which is usually placed at 5 times the RMS noise to avoid false signals) is ~250$e$. However, >1000 ions per second can be analyzed with single-pass CDMS,[48] making it the fastest CDMS technique. Therefore, single-pass CDMS is a useful technique for analytes outside the mass range of conventional MS when mass accuracy is not paramount. For example, size-exclusion chromatography (SEC) has recently been coupled to single-pass CDMS to characterize synthetic polymers.[57]

## Linear array CDMS

If an ion's charge is measured $N$ times, then the uncertainty is reduced by a factor of $n^{-1/2}$. One way to measure the charge multiple times is to pass the ion through a linear array of detector tubes and measure its charge in each one. Ions can still be analyzed fairly rapidly with this approach; measurements of 100 particles per s have been reported.[58]

Gamero-Castaño described the first linear array spectrometer in 2007; it contained six detector tubes (see Fig. 1).[59] If all the tubes are attached to the same amplifier, then the increased input capacitance limits the increase in performance, so the $n^{-1/2}$ scaling is not realized. Alternatively, if each detector tube is attached to a separate amplifier, then the charge uncertainty improves as desired, but the cost and complexity scales with $n$. Typically a compromise is reached, where one amplifier measures the signal from several tubes. In Gamero-Castaño's original work, two amplifiers were used,

 

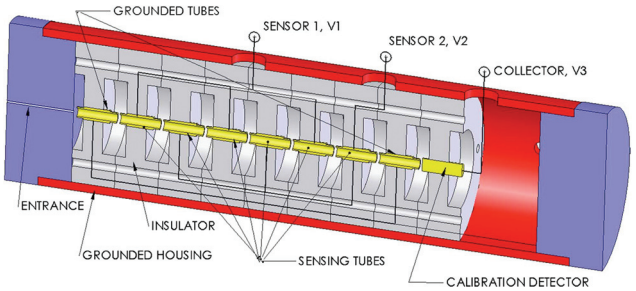


**Fig. 1** Schematic diagram of the linear array detector of Gamero-Castaño (from ref. 59).

each one connected to three detector tubes: one amplifier was connected to detectors 1, 3, and 5, and the other to detector 2, 4, and 6 (see Fig. 1). The largest reported linear array contained 22 detectors,[58] in which the first 11 detectors were connected to one amplifier, and the second 11 detectors were connected to a second amplifier.

There are three ways to analyze data in linear array CDMS. The simplest is the same approach used in single-pass CDMS, where an induced charge signal from an ion entering a detector tube rises above the noise, and its amplitude or area is used to determine the charge on the ion, while the flight time through the tube is used to determine the $m/z$. The charge uncertainty improves as the number of detectors increases; however, the limit of detection does not improve. The signal must still rise above the noise floor to be detected. A second approach is to do a fast Fourier transform (FFT) of the time domain data. This approach requires that the detector tubes are evenly spaced so the signal is periodic. The ion charge is determined from the magnitudes of the peaks in the FFT, and the $m/z$ is determined from the frequency of the fundamental, which is inversely proportional to the ion's velocity. With an FFT, both the charge uncertainty and limit of detection could in principle be improved further by increasing the number of detectors (if each detector has its own amplifier). As noted, however, the largest linear array reported has 22 detectors,[58] so there were not enough signal cycles for an FFT to be viable. The best results in linear array CDMS have been obtained with a correlation analysis of the data, where an ion signal is found by stepping an autocorrelation function across the time domain data, and the output of that analysis is correlated to the expected output pattern of an ion passing through the array. Using that methodology, an RMS charge uncertainty of $10e$ (five times better than single-pass CDMS) and a limit of charge detection of $100e$ (two times better than single-pass CDMS) have been achieved.[58] With that lowered limit of detection, ions as small as ~150 kDa were measured (over three times smaller than single-pass CDMS).

As with single-pass CDMS, the ion energy must be known to determine the $m/z$ from the velocity. Gamero-Castaño used an electrostatic mirror and only ions with a desired energy were deflected by the necessary angle to enter the detector array.[60] The disadvantage of this approach is that ions' with energies outside the accepted range are not analyzed, so substantial collisional cooling is needed to obtain a good ion signal. To analyze ions with a much broader range of energies, Smith *et al.* used a method similar to the pulsed acceleration method described above for single-pass CDMS. In their 22 detector array, the first 11 detector tubes were held at one potential, and the second 11 were held at a lower potential to decelerate the ions. The change in velocity was used to determine the ion energy.[58]

Austin and coworkers have created a linear array of charge detectors on a printed circuit board (PCB).[61] An array of metal film strips were printed on the PCBs and were used as electrodes. The PCBs are placed face-to-face with a small channel between them. An ion with high enough charge flying in between them will induce a detectable charge on the electrodes. So far, this approach is only proof-of-principle. Because the uncertainty in the charge measurement is reduced by a factor of $n^{-1/2}$ it is in principle possible to reduce the uncertainty to an arbitrarily small value by increasing the number of detectors ($n$). As noted above, the performance degrades when more than one detector is attached to each amplifier. Even if the expense and complexity of a large array could be tolerated, eventually the physical size will be limiting.

## Ion trap CDMS

In ion trap CDMS a detector tube is embedded in an electrostatic ion trap. The trapped ion oscillates back and forth through the detector allowing the charge to be measured multiple times.[62] The first ion trap CDMS measurements were reported by Benner in 1997. A cross section through Benner's trap is shown in Fig. 2a. The trap consisted of several flat, parallel electrodes on either side of a shielded detector tube. A plot of the electric potentials is shown in Fig. 2b. Ions oscillate back and forth through the detector tube in a potential "valley". To trap an ion the entrance electrodes are initially grounded to allow ions to enter the trap. When an ion enters the detector tube it induces a charge. If the resulting signal exceeds a predetermined threshold, the potentials on the entrance electrodes are raised and the ion is trapped. This mode of operation is called triggered trapping. The RMS noise on the detector was $50e$. The longest trapping time achieved in this study was about 10 ms (450 oscillations). According to Benner, the RMS uncertainty for one charge measurements is the RMS noise ($50e$), and given that the charge uncertainty improves by $n^{-1/2}$, the RMS uncertainty after 450 oscillations is reduced to $2.3e$.

Antoine and coworkers have recently used a similar trap.[63] A detector tube and an ion gate placed before the trap was used as a filter. If an ion's charge or $m/z$ were not in desired ranges as measured by the first detector tube, they were deflected by a potential on the ion gate and not allowed into the trap. Thus time is not wasted trapping ions that are not of interest. Ions were trapped for tens of msec.[19,20]

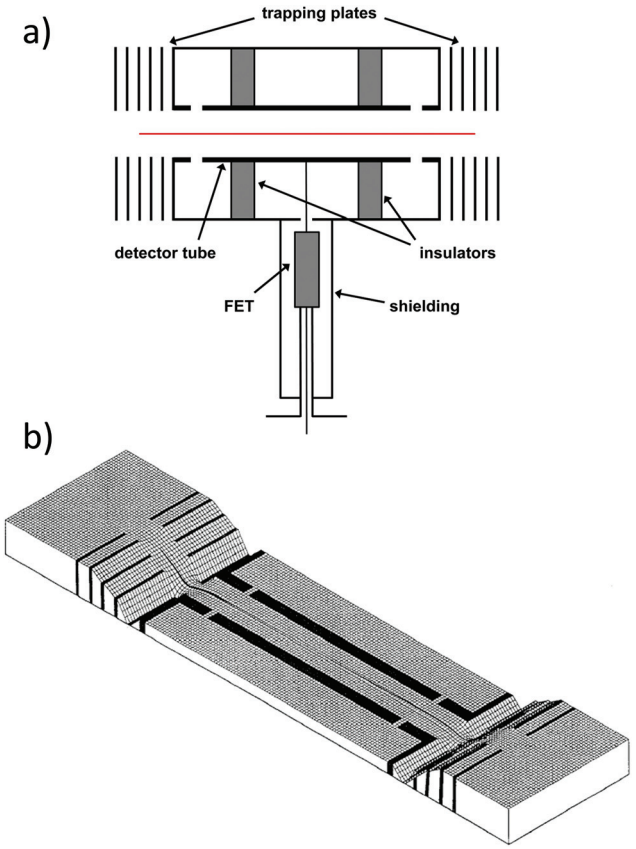


Fig. 2 (a) A schematic diagram of a cross section through Benner's electrostatic ion trap. (b) A three dimensional plot of the electric potentials in Benner's trap (adapted from ref. 62).

Inspection of Fig. 2b reveals that there are only weak restoring forces to push an ion back towards the central axis of the trap. As a result, ions are easily lost, and trapping times are relatively short. Longer trapping times lead to a lower uncertainty in the charge measurement, as well as a lower limit of detection. To increase trapping times, Contino and Jarrold used an electrostatic ion trap based on the cone trap design of Cederquist and coworkers.[64] A slice through the trap[65] is shown in Fig. 3. Equipotential lines are shown in red while the black line shows a trajectory of a trapped ion. The Lissajous-like pattern is typical for an ion that enters the trap off-axis, or with a trajectory that is not parallel to the trap axis. The stronger restoring force of the cone trap allows for much longer trapping times than the Benner-style trap. Ions have been trapped for 30 s. Such long trapping times require a background pressure in the UHV regime. Electrostatic ion traps only trap ions with a relatively narrow range of kinetic energies. With long trapping times, kinetic energy loss from collisions with the background gas can cause the ion energy to drop out of the range that is trapped and then the ion is lost.

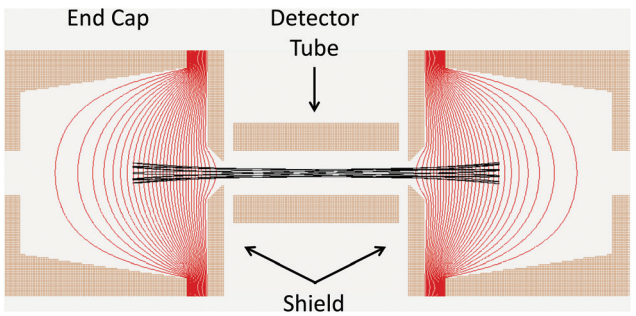


Fig. 3 Schematic diagram of the modified cone trap of Contino and Jarrold.[65] Equipotential lines are shown in red. The black line in the center shows part of a trajectory for an off-axis ion with a kinetic energy of 100 eV per $z$.

For ion trap CDMS using triggered trapping (where trapping events are triggered by the signal rising above the noise) the limit of detection is similar to single-pass CDMS. The threshold is usually set to around 5 times the RMS noise level.[62,63] Lower thresholds can be used but lead to an increase in empty trapping events (where trapping events are triggered by noise rather than an ion). The detection limit can be dramatically lowered using random trapping, where trapping potentials are periodically applied to the trap for a predetermined duration.[65] The time domain data for each trapping event is then analyzed by an FFT. If peaks in the FFT rise above a predetermined threshold, then one or more ions were trapped; otherwise, the trap was empty. A distinction between single ion and multiple ion trapping events can be made using harmonics (which are regularly spaced). Empty and multiple ion trapping events are discarded. Simulations indicate that when more than one ion is trapped, they interact, their trajectories are perturbed, and one of the ions usually leaves the trap after a short time. For single ion trapping events the $m/z$ is determined from the frequency of the fundamental peak, and the charge is determined from the magnitude of the peak. With random trapping, the limit of detection is improved by increasing the trapping time because the FFT peak magnitudes are proportional to trapping time ($t$) while the noise only rises with $t^{1/2}$. By trapping ions for about 400 ms, ions with charges as low as 6$e$ have been detected.[66] This lower limit of detection greatly expands the range of analytes that can be measured. With 30 s trapping it should be possible to detect single charges, though this has not been demonstrated because conventional MS methods are much faster than CDMS for light ions. Because of the low limit of charge detection with random trapping, CDMS spectra can be collected for relatively light, low-charged ions like cytochrome $c$.[67] This allowed for a direct comparison between the actual charge on the ions assigned by their $m/z$ values – as in conventional MS – and the charge measured by CDMS. All previous assessments of the charge accuracy were inferred from noise levels or simulations.

For triggered trapping, the average number of ions trapped per trapping event is given by

$$N_{\text{trapped}} = \overline{f_{\text{ion}}} \times t_{\text{capture}} \quad (1)$$

where $\overline{f_{\text{ion}}}$ is the average frequency that ions enter an open trap and $t_{\text{capture}}$ is the time that the ions spend in the trap during which they are trappable. $t_{\text{capture}}$ increases with $m/z$ because

 

more massive ions have lower velocities. With random trapping, there may be no ions, one, or multiple ions in the trap when a trapping event is initiated. The frequencies of empty, single ion, and multiple ion trapping events are given by a Poisson distribution:

$$f_{\text{empty}}^{\text{random}} = e^{-N_{\text{trapped}}} \times \frac{1}{t_{\text{trapped}}} \quad (2)$$

$$f_{\text{single}}^{\text{random}} = N_{\text{trapped}} e^{-N_{\text{trapped}}} \times \frac{1}{t_{\text{trapped}}} \quad (3)$$

$$f_{\text{multiple}}^{\text{random}} = [1 - e^{-N_{\text{trapped}}}(1 - N_{\text{trapped}})] \times \frac{1}{t_{\text{trapped}}} \quad (4)$$

where $t_{\text{trapped}}$ is the trapping time. Fig. 4 shows the frequencies of no ion (solid orange line), single ion (solid blue line), and multiple ion (solid red line) trapping events plotted against the average frequency that ions enter an open trap.

For triggered trapping, the frequency of single ion and multiple ion trapping events are given by

$$f_{\text{single}}^{\text{triggered}} = \left[\frac{1}{\frac{1}{f_{\text{ion}}} + t_{\text{trapped}}}\right] \times e^{-N_{\text{trapped}}} \quad (5)$$

$$f_{\text{multiple}}^{\text{triggered}} = \left[\frac{1}{\frac{1}{f_{\text{ion}}} + t_{\text{trapped}}}\right] \times (1 - e^{-N_{\text{trapped}}}) \quad (6)$$

In Fig. 4 the frequencies of single ion (dashed blue line) and multiple ion (dashed red line) triggered trapping events are plotted against the average frequency that ions enter an open trap. There are no empty trapping events with triggered trapping (unless the threshold is set too low).

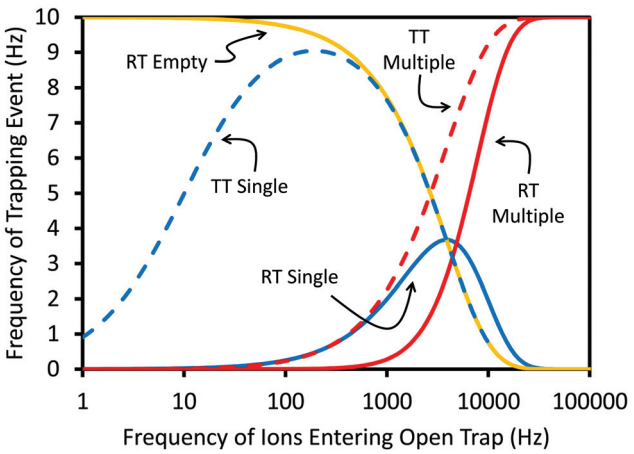


**Fig. 4** Plot of the frequency of trapping events *versus* the frequency of ions entering the modified cone trap shown in Fig. 3 for random trapping (solid lines) and triggered trapping (dashed lines). The results in the figure are for ions with an $m/z$ of 100 kDa (*i.e.*, 50 MDa, 500$e$ ions) and for a trapping time of 100 ms. The solid orange line (RT empty) is for events containing no ions (which only occur, in principle, for random trapping). The blue lines are for single trapping events. The dashed blue line is for triggered trapping (TT Single) and the solid blue line is for random trapping (RT Single). The red lines are for multiple ion trapping events. The dashed red line is for triggered trapping (TT Multiple) and the solid red line is for random trapping (RT Multiple).

Trapping events containing no ions are wasted time, and multiple ion trapping events cannot be analyzed because two highly charged ions trapped together interact and perturb the oscillation frequencies. Hence, only single ion trapping events are useful. The results in Fig. 4 were obtained for a trapping time of 100 ms (*i.e.*, a maximum of 10 trapping events per second). According to Fig. 4, the maximum frequency of single ion trapping events that can be achieved with random trapping is 3.7 Hz, and this requires an ion signal of around 4000 Hz. The frequencies in Fig. 4 depends on the ion's $m/z$. The results in the plot were obtained with an $m/z$ of 100 000 Da (a 50 MDa ion with a charge of 500$e$). Increasing the ion signal causes an increase in the fraction of multiple ion trapping events at the expense of the single ion events, and reducing the ion signal causes an increase in the fraction of empty trapping events at the expense of the single ion. The low single ion trapping efficiency (3.7 Hz *versus* 4000 Hz) results because the trap is closed for most of the time. Triggered ion trapping is considerably more efficient. The maximum frequency of single ion trapping events is around 9 Hz for a 100 ms trapping time, and this occurs for an ion signal of around 200 Hz. Triggered trapping is much more efficient than random trapping for sparse ion beams, but it is slightly less efficient for dense beams. In practice, triggered trapping should always be used for analytes that carry enough charge; the ion beam density can be controlled to maximize the frequency of single ion trapping events and minimize multiple ion events. However, random trapping is essential for analytes which do not carry enough charge to trigger a trapping event.

Increasing the trapping time reduces the uncertainty in the charge measurement by a factor of $t^{-1/2}$ (note that it is the trapping time and not the number of cycles that is the relevant parameter when FFTs are used to analyze the data). As noted above, the trapping time can be extended by optimizing the trap design and by operating in ultra-high vacuum to minimize collisions with background gas molecules.[68] Several other improvements have been made. First, cryogenically cooling the JFET at the input of the charge-sensitive preamplifier reduces thermal noise, which increases the signal-to-noise ratio.[67] Second, the signal from an ion oscillating in the modified cone trap is distinctly non-sinusoidal, and large, higher-order harmonics appear in the FFT of the signal.[68] Adding the magnitudes of the harmonics increases the signal-to-noise ratio over just using the fundamental peak. With all of the improvements, an RMS uncertainty of 0.20$e$ was achieved by trapping pyruvate kinase ions for ~3 s. For the first time, a charge spectrum measured by CDMS showed well-resolved peaks.[68] Because the charge states are resolved, the uncertainty can be reduced further by quantizing the charge (assigning the charge to the nearest integer value). Fig. 5a shows a plot (red line) of the root mean square deviation (RMSD) after quantization *versus* the RMSD before quantization. If the RMSD is greater than around 0.3$e$, quantization actually degrades the RMSD. This is because when the charges are quantized, some

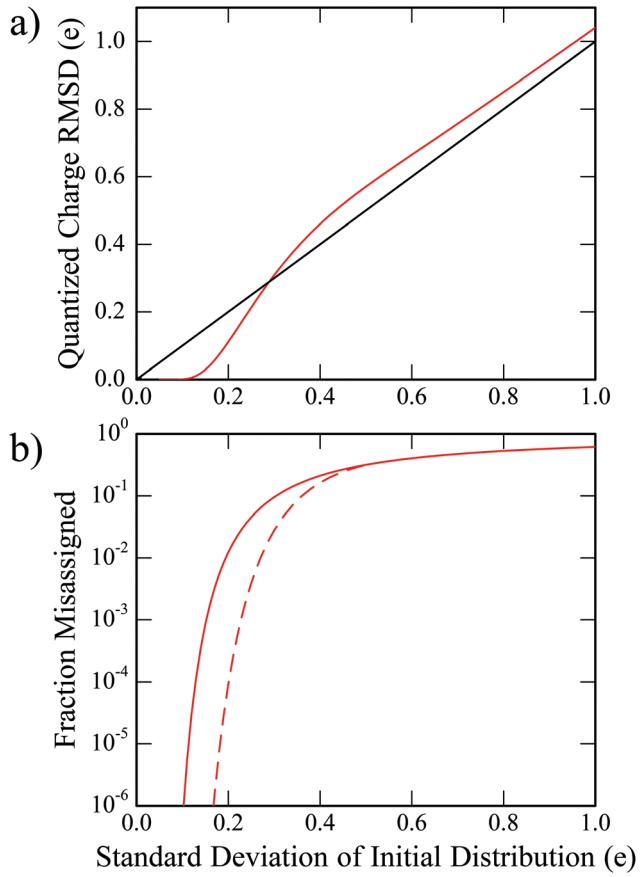


**Fig. 5** (a) Plot of the RMSD after quantization (red line) as a function of the RMSD of the initial distribution. A significant improvement in the RMSD is realized for distributions with an RMSD less than 0.3*e*. For initial distributions with an RMSD greater than 0.3*e*, quantization increases the RMSD because a substantial fraction of the ions are assigned to the wrong charge state. (b) Fraction of ions misassigned after quantization (solid red line) and after quantization and culling (dashed line). Culling removes ions with measured charges midway between two integer values. These ions are much more likely to be misassigned that ions with measured charges close to an integer value (from ref. 68).

ions can be assigned to the wrong charge state. However, for measurements where the RMSD drops below 0.3*e*, quantization can lead to a dramatic improvement (see Fig. 5a). For an initial RMSD of 0.2*e*, quantization lowers the RMSD to 0.11*e*. At this point it becomes more valuable to discuss the uncertainty in terms of the fraction of ions where the charge is misassigned. The solid red line in Fig. 5b shows the fraction misassigned plotted against the RMSD of the initial distribution. With an initial RMSD of 0.2*e*, the fraction misassigned is around 1%. This fraction can be dramatically reduced by discarding ions with measured charges close to half-way between two integers. Ions with measured charges midway between two integer values are much more likely to be misassigned than ions with measured charges close to an integer value. If ions more than one standard deviation from the center of the distribution are discarded, 32% of the ions are lost, but this includes 99.5% of the misassigned ones. The dashed line in Fig. 5b shows the improvement that is realized by culling ions more than one standard deviation from the center. For an initial RMSD of 0.2*e*, culling lowers the error rate from around 0.01 to $6.4 \times 10^{-5}$ (the RMSD is reduced to 0.008*e*). This corresponds to an error rate of just 1 in 15 000 ions, so for a typical ion trap CDMS measurement of a few thousand ions, the probability that all ions are assigned to the correct charge state is 80%. At that point, the remaining uncertainty in the mass measurement comes from the *m*/*z*, which is a reversal from early days of CDMS where the charge measurement was an order of magnitude less accurate than the *m*/*z* measurement. Unfortunately, the much-improved charge accuracy comes at the cost of speed. Each ion was trapped for 3 s and random trapping was employed. Therefore on average, the frequency of single-ion trapping events was only about 0.1 Hz. It is not always practical to take 10 s per ion to collect data. Other avenues to improve the charge accuracy would be to lower the noise on the detector further or to increase the energy of the ions. Increasing the ion energy (and the trapping potentials accordingly) would increase the oscillation frequency of an ion in the trap, reducing the 1/*f* noise.

Charge state resolution in a CDMS charge spectrum has not yet been achieved for more highly charged species for several reasons. The RMS charge uncertainty from noise is independent of charge, but it does depend on the frequency of the ion oscillation. Larger ions typically have higher *m*/*z* values, and hence lower oscillation frequencies. Therefore, the 1/*f* noise is higher. Also, deviations in an ion's energy or trajectory in the trap have small effects on the duty cycle, and that changes the magnitudes of the peaks in the FFT which in turn affects the charge measurement. Adding the magnitudes of the harmonics partially mitigates those changes in addition to improving the signal-to-noise ratio, but it does not completely remove them. The uncertainty in the charge measurement due to energy and trajectory issues scales with charge, so it is a more serious problem for very large ions.

Finally, the ion oscillation frequency depends on the ion energy, so the *m*/*z* measurement is also affected by ion energy. In this regard, it is important to collisionally cool the ions so that their kinetic energy distribution is narrow. Contino and Jarrold used a dual hemispherical deflection energy analyzer before the trap to filter out ions with kinetic energies per charge outside of a narrow range.[65] The trajectory of the ion in the trap also affects the oscillation frequency. For a particular *m*/*z* and kinetic energy, ions that oscillate along the trap axis have a slightly different frequency than ions that enter off axis. For long trapping times, collisions with the background gas affect the ion energy and influence the trajectory, causing the frequency to change with time.[11]

Williams and coworkers have recently reported results from an ion trap CDMS instrument with multiple detectors.[69] The configuration employed consisted of a cone trap with four detectors coupled to two amplifiers. The signals were processed using a pulse shaping amplifier to give a peak when the ion enters each cylinder and another when it leaves. The resulting time domain signals were sorted and processed

 

using a LABVIEW program. Mass distributions were measured for 50 nm and 100 nm polystyrene beads and for 8 MDa poly (ethylene oxide). Around 20% of the ions were trapped for more than 30 cycles. For these ions the uncertainty in the charge measurement was around 1%, based on the standard deviation of the mean for the multiple measurements. The multiple detector configuration may offer some benefits over the single detector ion trap, but there are also costs (for example, increased size and complexity). Whether the multiple detector configuration will significantly outperform the single detector ion trap remains to be seen.

## Side by side comparison of the CDMS variants

The three instrumental variations on the CDMS theme have their own strengths and weaknesses. Single-pass CDMS is the least accurate and has the highest limit of detection, but it is much easier to implement than the other methods, and data can be collected much more quickly. Ion trap CDMS is by far the most accurate, and it has by far the lowest limit of detection when operated in the random trapping mode, but data collection is much slower, and painfully slow for very long trapping times. Linear array CDMS strikes a balance between speed and accuracy. Table 1 summarizes some of the main figures of merit for the three techniques. All values shown are the best that have been obtained experimentally, rather than what is theoretically possible.

## Applications of CDMS

In what follows we summarize measurements that have been performed with CDMS, highlighting the findings and the impact on the application field of interest. Some of the first modern electrospray-based CDMS measurements were of polynucleotides by Benner and co-workers in the 1990s. Later, measurements were performed for viruses and protein assemblies. Finally, CDMS has also been applied to the study of nanoparticles and synthetic polymers.

**Table 1** Figures of merit for different varieties of CDMS. Values are what has been achieved experimentally, not what is theoretically possible. For Ion trap CDMS values are given for three different trapping times

| Technique | Rate (ions per s) | RMS uncertainty ($e$) | Limit of detection ($e$) |
|---|---|---|---|
| Single-pass | 1000 | 50 | 250 |
| Linear array | 100 | 10 | 100 |
| Ion trap | 4 (100 ms trapping) | 1.3 | 13 |
| | 1 (400 ms trapping) | 0.65 | 7 |
| | 0.1 (3 s trapping) | 0.2 (0.008)[a] | —[b] |

[a] With quantization of the measured charges and culling of ambiguous ones. [b] Not investigated, but the limit of detection should scale with the square root of the trapping time so a value of around 3 is expected.

## DNA and RNA polynucleotides

Fuerstenau and Benner demonstrated the potential of CDMS for the analysis of polynucleotides; first with a single-pass experiment,[44,45] and later with ion trap CDMS.[62] With single pass CDMS, the molecular weights of several DNA polynucleotides of known molecular weight (between 2.8 and 31 MDa) were recorded, though with insufficient mass resolution to make the technique immediately competitive with the electrophoretic measurements carried out at that time. However, CDMS analysis of DNA ions provided information that is not obtained by alternative methods: a correlation of the ions' charge and mass can provide information on the shape of the ion. For example, a scatter plot of charge *versus* mass for 31.5 MDa Lambda Phage DNA is linear. This result suggests that the ions adopt an extended conformation as they accumulate charge during the electrospray process. This result may also provide clues about the electrospray mechanism for analytes with dimensions significantly larger than the primary electrospray droplet. How does a 16 μm DNA strand pick up charge during the electrospray process? Though the answer to this intriguing question is out of the scope of this review, it demonstrates the advantage of having directly coupled mass and charge information for individual ions and the inferred structural information it provides.

Benner's gated trap measurements were performed for a 4.3 kb circular plasmid with a theoretical mass of 2.69–2.88 MDa depending on the number of sodium adducts associated with the phosphate backbone. Of note, the DNA was dissolved in Tris-HCl buffer, which is considered incompatible for ESI-MS analysis due to the potential for electrospray ion suppression, and mass heterogeneity due to salt adduction. Salted DNA ions were analyzed by MS in this experiment to provide a more direct comparison of the gel-based and CDMS techniques. The repetitious measurements in the trap afforded higher mass resolution (5× improvement over the single-pass instrument) that rivals gel-based separations for DNA that has not been desalted. Benner also pointed out the time advantage of CDMS: a gel separation took 4 hours of analysis time, and analysis by CDMS took less than 10 minutes. Still, higher resolution capillary electrophoresis (CE) techniques have since been developed.[70] Benner has suggested that CDMS could rapidly measure the length of overlap produced from the cloning process during sequencing as this process is complex and often avoided when utilizing CE. He also suggests the use of CDMS to identify and sort chromosomes as a more accurate alternative to fluorescence-based methods. Schultz, Hack and Benner have used single-pass CDMS to analyze products of polymerase chain reaction (PCR) between 1525 and 2677 base pairs in length.[46] Again, with limited mass resolution from the single-pass charge detection measurement, the advantage presented here was the improved timescale of the measurement and the ability to measure products without extensive sample preparation.

More recently, Dugourd and coworkers have published a series of papers demonstrating the use of CDMS to study the

photofragmentation of single DNA macromolecules.[19,20,63,71] This work illustrates the use of ion trap CDMS as a method to study the properties of individual gas-phase ions. Specifically, infrared multiphoton dissociation was employed to enable efficient fragmentation of DNA macromolecules in the megadalton size range. Examples are shown in Fig. 6 for the photofragmentation of single ds/circular M13mp18 ions. For these experiments, the signal was processed with a Gaussian differentiator which yields a positive going pulse when the ion enters the detector tube and a negative going pulse when it leaves. The amplitude of the pulses provides the charge. In the examples shown in Fig. 6, the charge starts at around 800–1000*e*, and then somewhere between 5 and 10 ms it decreases as the ion dissociates and the fragments are ejected from the trap. The signal at the end of the trapping time (after the ion has left the trap) is due to noise. Using this approach, relative activation energies for the unimolecular dissociation of single DNA ions were determined and were found to increase as a function of molecular weight. These measurements are of particular interest because the single-particle nature of the studies uncovered fragmentation pathways that would not be detectable in an ensemble study.[71] Three specific pathways of dissociation were observed, based on the shape of the induced charge waveform as a function of time. Examples of the three pathways are shown in Fig. 6. "Sudden loss" type pathways were characterized by a sharp decrease in measured

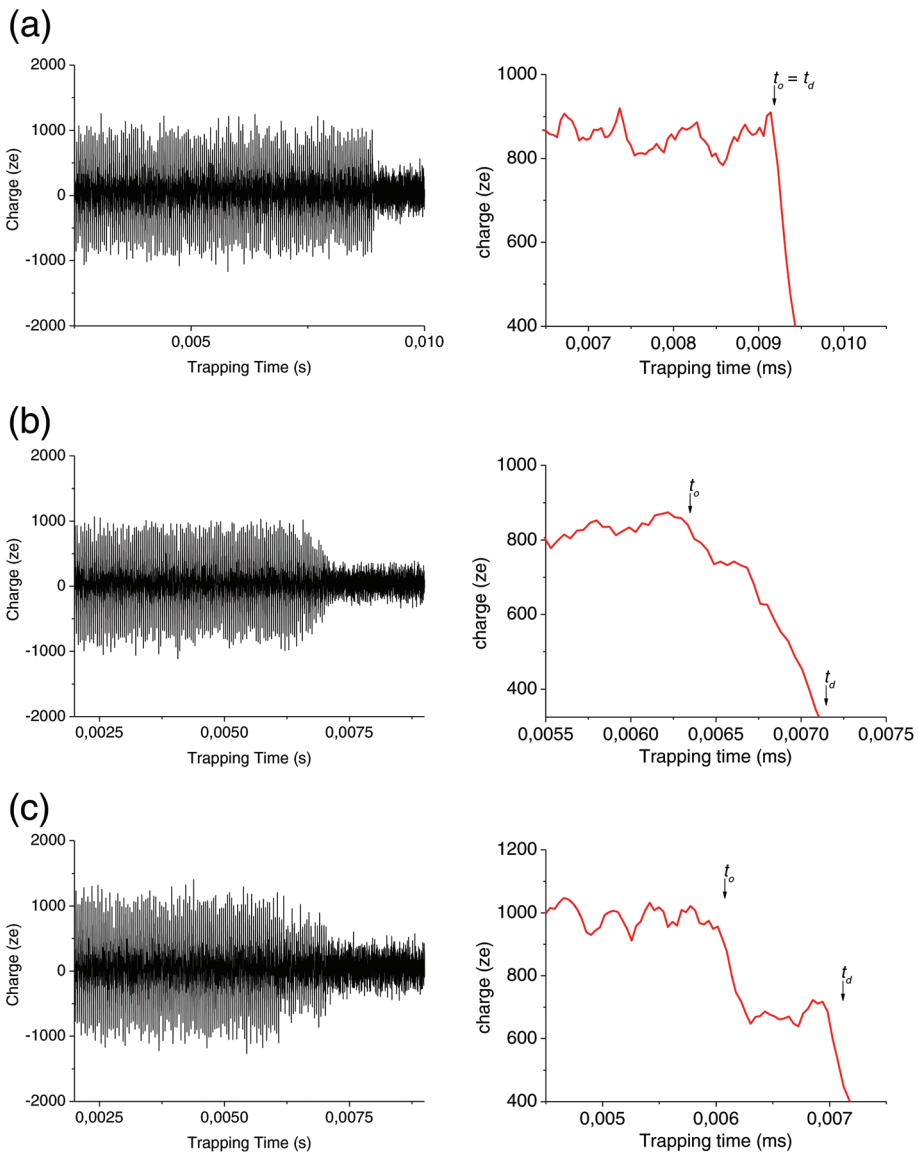


**Fig. 6** The plots on the left show examples of waveforms for single trapped ds/circular M13mp18 ions irradiated at 6.4 W cm$^{-2}$. Three different types of dissociation behavior are highlighted: (a) "sudden-loss", (b) "funnel", and (c) "staircase". The plots on the right show the evolution of the number of elementary charges as a function of time. The raw data was smoothed by averaging over 10 adjacent points. The onset time ($t_o$) (when dissociation starts) and disappearance time ($t_d$) are also indicated for each waveform (from ref. 20).

 

signal and are attributed to dissociation events where the fragment ion is lost from the trap (Fig. 6a). "Funnel" type pathways are characterized by a more gradual loss of charge (Fig. 6b) and "staircase" type pathways are characterized by loss of charge followed by periods where the charge remains constant (Fig. 6c). The latter pathways were more dominant for non-hybridized double stranded DNA that is not fully base-paired; this may be a sign of partial fragmentation or partial unzipping of the strands.[19] Generally, hybridized double-stranded DNA was found to have higher activation energies than non-hybridized dimers which likely reflects the higher degree of base pairing in the hybridized strands. Lower mass fragments (with charges below 400*e*) were not detected because of the relatively high limit of detection in these studies (400*e*).

## Protein assemblies

Improvements in CDMS instrumentation and methods have allowed the detection of small proteins with relatively low charges.[65–67] These results are significant because they indicate that CDMS can be used to monitor masses over a very broad range which might be encountered in assembly or fragmentation reactions involving large ions. Pyruvate kinase (PK) exists as a 232 kDa tetramer that forms higher order multimers under non-denaturing conditions.[72] Fig. 7 shows the *m*/*z* and CDMS mass spectra of PK.[73] In the conventional TOF *m*/*z* spectrum (Fig. 7a), charge state envelopes for the PK tetramer, octamer, and dodecamer are observed along with unresolved distributions at higher *m*/*z* values. With the same electrospray and source conditions, the CDMS spectrum reveals multimers up to the 40-mer (10 PK tetramers, see inset in Fig. 7b). From measurement of the multimer abundances as a function of PK concentrations, it was suggested that the multimers resulted from non-specific aggregation in solution.[73]

Recently, Doussineau *et al.* showed that CDMS is capable of measuring masses of amyloid fibrils.[74] Previous MS-based studies of fibrilation have been limited to the early steps in aggregation.[75] The CDMS measurements provided rapid access to information like average mass and polydispersity index, and when coupled with measurements of the average length of the fibrils from AFM, the mass per unit length (MPL) was determined. The MPL values were consistent with fibril strands comprised of more than one filament. The mass and length distributions are log-normal which is characteristic of non-specific aggregation. The fibrils were reported to be up to 50 μm long, much larger than typical electrospray droplets, so these studies also raise interesting questions about how such a long object is transferred into the gas phase by electrospray. For example, do some of the fibrils break due to mechanical forces during this process? The CDMS measurements were performed in the single pass mode and the RMS detector noise was 150*e*. The measured charges ranged from around 300*e* to 2500*e*. The relatively high uncertainty in the charge measurements leads to a relatively low mass resolving power ($M/\Delta M$) of 4–8. With the instrumental advances described above, in particular the much lower limit of detection and higher charge accuracy, it should be possible to monitor protein aggregation and fibrillation reactions in real time using CDMS.

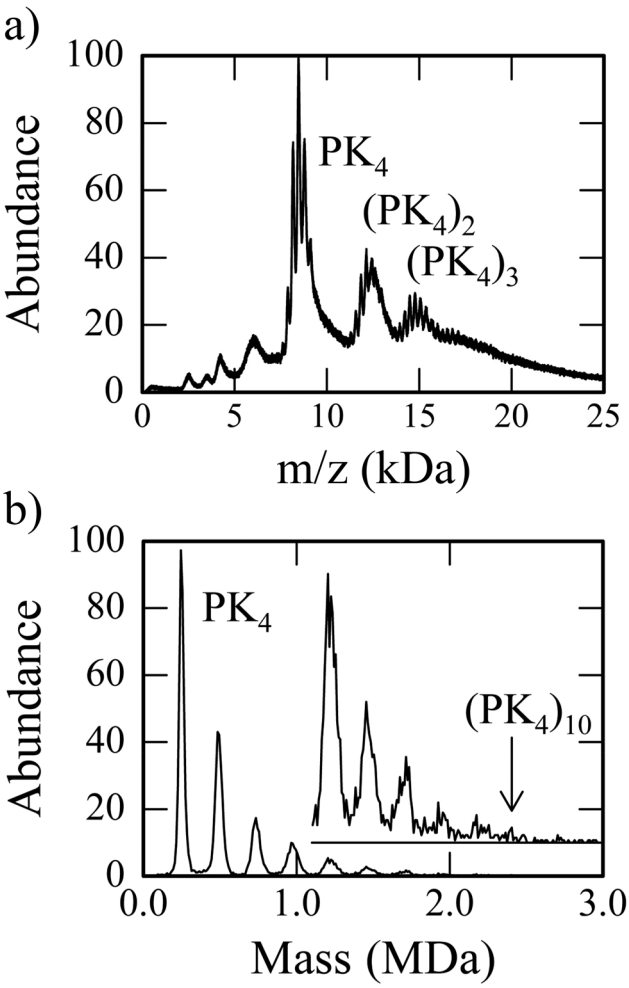


**Fig. 7** Comparison of (a) *m*/*z* spectrum measured by TOF-MS and (b) mass spectrum measured by CDMS for pyruvate kinase (PK). In the TOF-MS *m*/*z* spectrum higher order multimers are not resolved (adapted from ref. 73).

## Viruses

Siuzdak and coworkers were the first to show that viruses could successfully survive electrospray and the gas expansion into vacuum.[76,77] In their experiments, a brass collection plate was inserted in the ion path. After electrospray and deposition of the virus samples, the plate was removed from vacuum and analyzed by transmission electron microscopy. The images showed that the viruses retained their shape, spherical for Rice Yellow Mottle Virus (RYMV) and rod-like for Tobacco Mosaic Virus (TMV).

Fuerstenau *et al.* were the first to measure masses of intact viruses.[47] These measurements were performed by single-pass

CDMS. The measured masses of RYMV (6.5 MDa) and TMV (40.5 MDa) matched the expected masses, but the mass distributions were very broad due to uncertainty in the charge measurements. Differences in the charges of rod-like TMV and icosahedral RYMV were noted.

## Hepatitis B virus and woodchuck hepatitis virus

Virus capsids are often assembled from hundreds of identical proteins. About half of known virus families have icosahedral capsids. The arrangement of the subunits in an icosahedral capsid can be described by its triangulation number, or $T$ number.[78] The $T$ number also provides the number of coat proteins making up the capsid, which is $60 \times T$. Only certain $T$ numbers are valid; the lowest ones are $T$ = 1, 3, 4, and 7. Capsid assembly is a target for antiviral drug development, and understanding the mechanism of the assembly reaction is an important scientific problem. Detection of intermediates along the assembly pathway is difficult because intermediates are transient and present at very low concentrations.[79] Conventional MS has identified early intermediates in some cases,[80] but late assembly intermediates have been elusive. One way to identify intermediates is to create kinetic traps by running the assembly reactions under conditions where many nuclei are formed and there is insufficient capsid protein to complete them. For Hepatitis B virus (HBV) this scenario can be realized with high ionic strength. Several trapped, late-assembly intermediates have been detected using CDMS.[81] Fig. 8a shows the CDMS spectrum measured for HBV assembled under low ionic strength (300 mM NaCl). The peak at around 3 MDa is due to the $T$ = 3 capsid with 90 capsid protein dimers and the peak at around 4 MDa is due to the $T$ = 4 capsid with 120 dimers (the capsid protein dimer is the building block for the HBV capsids). Fig. 8b shows the spectrum measured for high ionic strength (1 M NaCl) assembly where there are trapped intermediates with masses between the $T$ = 3 and $T$ = 4 peaks. The mass resolution is insufficient to resolve intermediates with a specific number of dimers; however, the prominent intermediates at 3.5 and 3.7 MDa are missing 9–10 and 15–16 dimers. Cryo-EM images suggest that the intermediates are incomplete $T$ = 4 capsids (*i.e.* $T$ = 4 capsids with a hole).

CDMS has also been used to study capsid–protein interactions. In one study, the number of importin β molecules bound to HBV capsids was measured. Importin β is a ~10 kDa protein involved in transporting mature HBV capsids to the cell nucleus. Cryo-EM reconstructions indicate that the C-terminal domain that binds importin β extrudes through the capsid and interacts with free protein. CDMS was able to quantify the number of importin β complexes bound to a single capsid. Titration experiments showed that the number bound was sensitive to ionic strength and that capsids could be saturated. However, the number of importin β at saturation was well beyond the expected number based on capsid morphology. Further cryo-EM studies revealed that high concentrations of importin β destabilize HBV capsids and become internalized.[82]

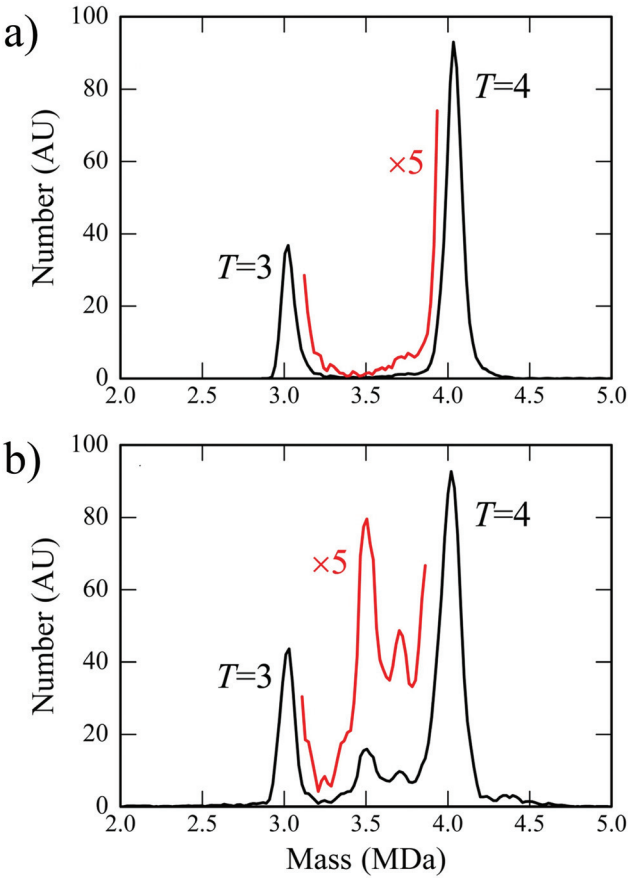


**Fig. 8** CDMS spectrum measured for Hepatitis B virus (HBV) capsids assembled under (a) low ionic strength (300 mM NaCl) and (b) high ionic strength (1 M NaCl). The low ionic strength spectrum is dominated by peaks at around 3 and 4 MDa which are attributed to the $T$ = 3 and $T$ = 4 capsids of HBV. With high ionic strength, trapped intermediates with masses around 3.5 MDa and 3.7 MDa are apparent (adapted from ref. 83).

Woodchuck Hepatitis Virus (WHV) is a close relative of HBV. However, their assembly behaviors are quite different.[83] WHV forms a broad array of oversized, aberrant particles which are challenging to characterize both because of their large size and their heterogeneous nature. CDMS measurements showed only around 50% normal capsids and a broad distribution of oversized capsids with prominent peaks at certain sizes (such as 150 capsid protein dimers).[84] Certain prominent peaks in the oversized capsid distributions could be explained by hexameric defects that lead to elongated capsids;[85] however, others could not be explained by theoretical predictions. Cryo-EM analysis confirmed the presence of normal capsids and elongated capsids, but also capsids that were not properly closed and formed "spiral-like" morphologies, perhaps explaining the observed heterogeneous mass distribution.

 

## Adeno-associated virus vectors for gene therapy

Adeno-associated virus (AAV) is a promising vector for gene therapy because it is non-pathogenic and because viral serotypes target tissues relevant to the treatment of specific diseases. AAV capsids are assembled and subsequently package single-stranded DNA. A fraction of AAV particles do not package DNA and are therefore unable to act therapeutically. In proof-of-principle studies, CDMS was used to measure relative quantities of full and empty particles (*i.e.* ones with and without DNA, respectively) in AAV vector preparations.[86] CDMS was also able to detect capsids that have packaged partial genomes, which are also considered "unwanted" particles from a gene therapy perspective. Fig. 9 shows the CDMS spectrum measured for a preparation of AAV8 (AAV serotype 8) with an sc-GFP genome. The peak at around 3.7 MDa is due to the empty capsid and the peak at around 5.1 MDa is due to the capsid with the whole genome. The broad peak centered on around 4.4 MDa is due to packaging of a partial genome. The maximum in this peak lies around halfway between the peaks due to the empty and full capsids and this indicates a tendency to cleave the DNA at its midpoint. The small peak centered on around 5.6 MDa is due to an impurity of unknown origin.

## Bacteriophage P22

Bacteriophage P22 is a *Salmonella*-infecting, double-stranded DNA virus weighing over 50 MDa. P22 is large (65 nm diameter) and *in vivo* assembly requires scaffolding proteins to achieve a capsid with the correct morphology. A procapsid is an immature form of P22 that consists of capsid proteins and internal scaffolding proteins. CDMS was used to measure the average number and distribution of scaffolding proteins encapsidated within P22 procapsids.[87]

P22 normally assembles into a $T = 7$ capsid. Single amino acid substitutions to the coat protein can dramatically affect capsid assembly, leading to "petite" capsids.[88] CDMS was used to investigate the particles assembled from A285Y and A285T variants.[89] Fig. 10a shows the CDMS spectrum measured for the A285T variant coat protein after assembly, treatment with guanidine hydrochloride to remove scaffolding protein, and cross-linking with formaldehyde. Without cross-linking many of the capsids are broken-up during electrospray and the transition into the instrument. The vertical blue lines show the expected masses of the empty $T = 1$, 3, 4, and 7 capsids. There are sharp peaks close to the expected masses for the empty $T = 4$ and $T = 7$ capsids. Fig. 10b shows a scatter plot of charge *versus* mass for the ions in Fig. 10a. Each point represents the charge and mass of a single ion. Large ions generated by elec-

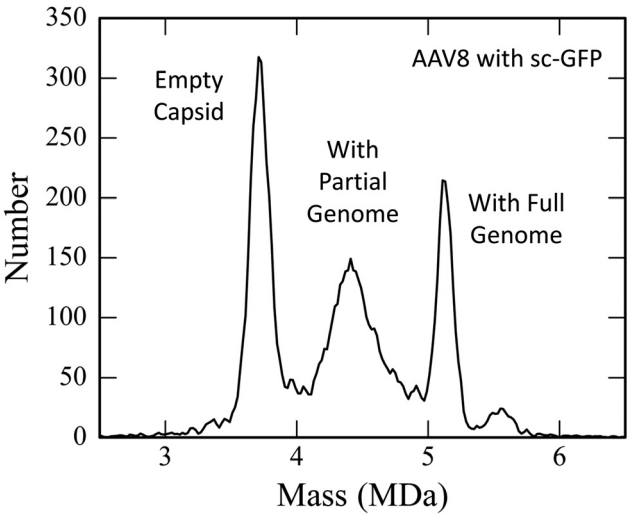


**Fig. 9** CDMS spectrum measured for adeno associated virus with an sc-GFP genome. The peak at 3.7 MDa is due to empty capsid and the peak at 5.1 MDa is due to capsid that has packaged the full genome (adapted from ref. 86).

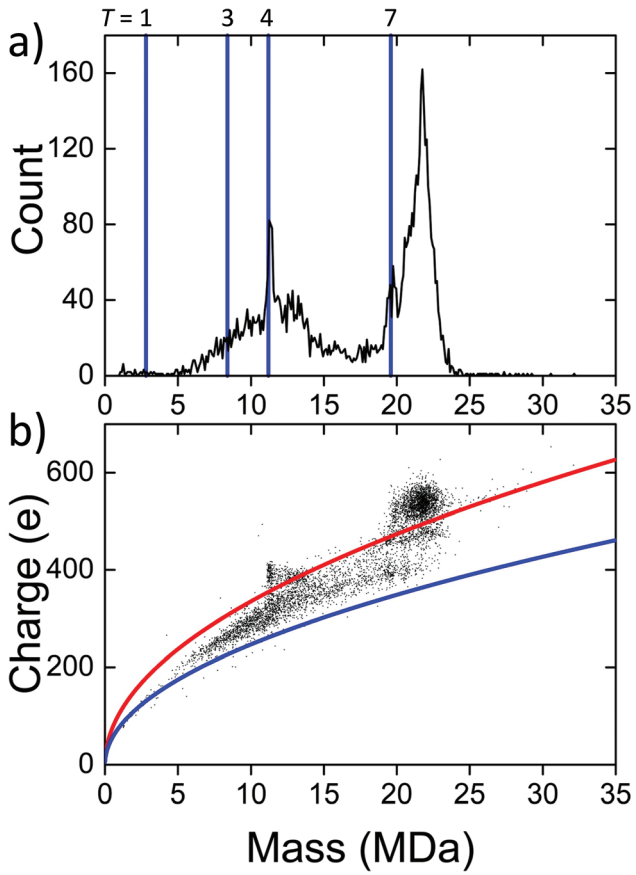


**Fig. 10** (a) Mass distribution measured by CDMS for P22 procapsids assembled from A285T variant coat protein after treatment with guanidine hydrochloride to remove scaffolding protein and cross linking with formaldehyde. The blue vertical lines show the expected masses for capsids with $T = 1$, 3, 4, and 7. (b) Charge *versus* mass scatter plot for ions in the mass spectrum in (a). The blue line shows the Rayleigh limit for globular proteins (see text) and the red line shows this limit scaled up to separate the more highly charged clusters of ions from the lower charged background (adapted from ref. 89).

trospray are expected to be charged to 70–100% of the Rayleigh limit[90] for a water droplet of the same diameter as the analyte.[91] The blue line in Fig. 10b shows the Rayleigh limit for globular proteins[92] and the red line shows the Rayleigh limit scaled-up so that it separates the more highly charged clusters of ions from the lower charged background. The highly charged clusters above the red line are attributed to empty, or nearly empty, capsids. They have larger diameters than globular structures of the same mass which leads to their higher charge. On this basis, the large broad peak in Fig. 10a at masses larger than expected for the empty $T = 7$ is also attributed to capsids. These may be $T = 7$ capsids that have retained some scaffolding protein. The ions with charges below the red line are partially collapsed, presumably because the variant proteins did not assemble into the correct, stable structures.

The mature P22 phage consists of the capsid, the tail machine, ejection proteins, and a double-stranded genome which is actively packaged by the headful mechanism. Altogether, it is believed to contain 521 copies of 9 different proteins plus the genome. The theoretical mass, obtained by adding the masses of the components in the predicted stoichiometry, is 51 613 585 Da. Despite its enormous size and complexity, P22 phage survives the transition into the gas phase. Keifer *et al.* recently used CDMS to measure the accurate mass of the mature phage.[93] The measured value, 52 180 ± 59 kDa, is 1.1% larger than the theoretical mass. Electrospray from non-denaturing solvents is known to lead to measured masses that are slightly larger than the theoretical mass due to adduct formation with salt, counter ions, and solvent.[5] The deviation found here is consistent with previous measurements on smaller protein complexes by conventional mass spectrometry. The width of the peak in the mass distribution can provide important information about heterogeneity. The measured peak had an intrinsic full width at half maximum (FWHM) of 747 ± 66 kDa. The headful mechanism leads to a distribution of packaged DNA that can entirely account for the intrinsic FWHM of the measured peak. This suggests that there is little heterogeneity in the stoichiometry of the protein components.

## Nanoparticles and polymers

CDMS is not limited to the study of biological macromolecules. It has also been used to study nanoparticles,[51] amphiphilic block copolymer micelle particles,[49,50] poly(ethylene oxide),[48,58] and copolymer vesicles[53] with mass distributions extending into the gigadalton mass range. Mass and charge information obtained from CDMS measurements has been used to calculate size distributions and deduce information about morphology. These studies demonstrate that CDMS is a valuable tool which can provide better or orthogonal information to established characterization techniques such as light scattering, electron microscopy, and X-ray scattering.

Mass and charge distributions for poly(ethylene oxide) (PEO), also known as polyethylene glycol, have been measured by Smith *et al.*,[58] Elliot *et al.*,[69] and Doussineau *et al.*[48] at the Université de Lyon. Smith *et al.* measured the mass and charge distributions of 300 kDa PEO ions by linear array CDMS. Elliot et al used ion trap CDMS to measure 8 MDa PEO and the Lyon group used single pass CDMS to measure mass and charge distributions for several different sizes of PEO (nominally 1, 2, 4, and 6 MDa).[48] In all cases, the resulting mass distributions were broad, as expected from the polydispersity index of PEO prepared by heterogeneous catalysis. The maxima were in good agreement with the expected masses. Doussineau *et al.* used the charge state information to study the influence of alkali cations on the charging capacity of PEO and found that the high molecular weight polymers do not adopt fully extended conformations. As a follow-up, the Lyon group coupled SEC to CDMS to quickly and efficiently generate an SEC calibration curve from the polymer analyte itself (polyacrylamide and other polymers were used), as opposed to calibration from non-related, external standards.[57]

The Lyon group also used a single-pass CDMS to determine the mass of polymeric nanoparticles, comprised of self-assembled amphiphillic block copolymers.[49] Previous attempts to determine the size of these nano-sized polymers used dynamic light scattering and TEM, which tend to overestimate and underestimate size, respectively. The measured mass distributions of the various preparations of polymer nanoparticles were relatively broad, monomodal distributions. The width of the peaks was attributed to the variability in the number of polymers in the particles. The ability to characterize synthetic polymer particles by mass and polydispersity may help drive advances in copolymer particle synthesis for biomedical and materials applications.

Amphiphilic block copolymer nanoparticles were also used to investigate the charging mechanism of electrospray ionization for macromolecular, spherical particles in the mega and gigadalton size range.[50] The findings show that the nanoparticles, weighing between 500 and 2000 MDa charge to roughly 60–65% of the Rayleigh limit. The authors show that charging can be increased by the addition of supercharging agents such as piperdine, which may disrupt the micellar structure and result in larger, more highly charged particles.

The Lyon group has used electrospray-CDMS to investigate the relationship between charging in the solution and gas phases.[52] Specifically, the charging of negatively and positively charged polymeric nanoparticles were measured and compared to results obtained from solution-based zeta potential measurements. The measurements show a correlation between the solution and gas phase charges (Pearson correlation coefficient of 0.89). Thus it may be feasible to use the gas-phase measurement to characterize nanoparticle charge. Mathematical treatment of the nanoparticle molecular weight, solution phase charges by zeta potential measurements, and the gas-phase measurements demonstrate that the charge distributions in solution and in the gas phase are correlated independently of the size of the particle and provides insight into the charging mechanism of polymeric nanoparticles.

Two final examples of CDMS analysis of nanoparticles by the group at Lyon involved the morphological characteriz-

 

ation.[51,57] In those studies, CDMS was used in tandem with other physical characterization techniques such as SAXS, TEM, and DLS, to characterize polymerization-induced self-assembly of vesicle particles and nanoparticle clusters. For the vesicle particles, CDMS data helped further understanding of vesicle growth during the self-assembly process, including the point where the vesicles "self-destruct" due to the gradual ingress of water into the vesicle membrane. Comparison of CDMS and SAXS data shows good agreement, though the calculated particle diameters and vesicle membrane thicknesses calculated from CDMS information are lower than those reported by both SAXS and DLS, probably due to the dehydration that occurs in vacuum. For the composite nanoparticles, CDMS was used characterize the size, size distributions, shapes, and surface areas, and compared with similar results obtained by TEM. Tetrapod, hexapod, and dodecapod configurations, produced by a controlled polymerization process, were studied. The CDMS results indicate that there were several subpopulations for each morphology. The mass resolution of the instrument was insufficient to resolve the subpopulations, so a mathematical deconvolution of the data was performed. The relative proportions of the cluster subpopulations determined by CDMS was in good agreement with those determined by TEM.

## Summary and prospects

CDMS extends the reach of mass spectrometry into the gigadalton regime. It also allows the analysis of very heterogeneous samples. Mixtures of high mass species confound conventional MS methods because of the large number of overlapping charge state sequences. Single pass CDMS measurements are fast but inaccurate while ion trap CDMS is slow but much more accurate. Linear array CDMS lies in between in terms of accuracy and speed. The uncertainty in the mass measurement for each ion is a combination of the uncertainties for the charge and $m/z$ measurements. In early work the poor accuracy of the charge measurement was limiting. The charge can now be measured with almost perfect accuracy and the current concern is with the length of time required to make the measurement. The measurement time can be reduced by increasing the signal to noise ratio (SNR), and the scaling in this regard is favorable: doubling the SNR allows to a four-fold reduction in the trapping time for the same uncertainty. The accuracy of the $m/z$ measurement is another area in need of improvement.

Along with the technological developments of the last few years, there has been an increase in the breadth of application. There are many examples now of the value of CDMS in obtaining information that cannot be obtained by conventional MS or by any other technique. The applications can be loosely divided into two main groups: applications where the goal is to determine the mass distribution of a very heterogeneous sample (*e.g.*, polymers, nanoparticles, and amyloid fibrils) and applications where the goal is to determine stoichiometry (*e.g.*, assemblies, protein complexes, viruses, and virus assembly intermediates). In the former, the accuracy of the mass measurement is not paramount and single pass CDMS could be used, although linear array CDMS or ion trap CDMS with a short trap time would be better. When stoichiometry is the goal, resolution and mass accuracy are important. In cases where supramolecular assemblies contain multiple subunits a single mass measurement alone may not be enough to define the stoichiometry (particularly if some of the subunits are unknown). In these cases, one way forward is to combine CDMS with MS/MS methods. Selected assemblies are dissociated and then the fragments are analyzed by CDMS.

At present, CDMS can provide rudimentary size and structural information from a correlation of the charge and mass measurements, but only in limited circumstances. For example, as discussed above, CDMS can distinguish between ion morphologies when multiple charge distributions are present, or it can provide the size of the analyte if the density is known. However, in most cases it cannot provide absolute structural information. The combination of ion mobility with CDMS would therefore be beneficial, allowing access to more detailed size and shape information for very large ions. Coupling ion mobility with CDMS appears feasible but not straightforward. All three variants of CDMS could be coupled to other separation techniques although the higher throughputs of the single-pass and linear array approaches make them the most attractive, at least for applications where mass accuracy and resolution are not critical.

## Acknowledgements

We are grateful for the support of the National Science Foundation through award CHE-1531823.

## References

1 J. Snijder, R. J. Rose, D. Veesler, J. E. Johnson and A. J. R. Heck, Studying 18 MDa Virus Assemblies with Native Mass Spectrometry, *Angew. Chem., Int. Ed.*, 2013, **52**, 4020–4023.
2 I. S. Gilmore and M. P. Seah, Ion Detection Efficiency in SIMS: Dependencies on Energy, Mass and Composition for Microchannel Plates Used in Mass Spectrometry, *Int. J. Mass Spectrom.*, 2000, **202**, 217–229.
3 G. Westmacott, M. Frank, S. E. Labov and W. H. Benner, Using a Superconducting Tunnel Junction Detector to Measure the Secondary Electron Emission Efficiency for a Microchannel Plate Detector Bombarded by Large Molecular Ions, *Rapid Commun. Mass Spectrom.*, 2000, **14**, 1854–1861.
4 G. W. Fraser, The Ion Detection Efficiency of Microchannel Plates (MCPs), *Int. J. Mass Spectrom.*, 2002, **215**, 13–30.
5 P. Lössl, J. Snijder and A. J. R. Heck, Boundaries of Mass Resolution in Native Mass Spectrometry, *J. Am. Soc. Mass Spectrom.*, 2014, **25**, 906–917.

6 A. V. Loboda and I. V. Chernushevich, Investigation of the Mechanism of Matrix Adduct Formation in MALDI at Elevated Pressure, *Int. J. Mass Spectrom.*, 2005, **240**, 101–105.
7 S. F. Wong, C. K. Meng and J. B. Fenn, Multiple Charging in Electrospray Ionization of Poly(Ethylene Glycols), *J. Phys. Chem.*, 1988, **92**, 546–550.
8 P. G. Stockley, O. Rolfsson, G. S. Thomspon, G. Basnak, S. Francese, N. J. Stonehouse, S. W. Homans and A. E. Ashcroft, A Simple, RNA-Mediated Allosteric Switch Controls the Pathway to Formation of a $T = 3$ Viral Capsid, *J. Mol. Biol.*, 2007, **369**, 541–552.
9 J. Bereszczak, M. Havlik, V. Weiss, M. Marchetti-deschmann, E. Duijn, N. Watts, P. Wingfield, G. Allmaier, A. Steven and A. R. Heck, Sizing Up Large Protein Complexes by Electrospray Ionisation-Based Electrophoretic Mobility and Native Mass Spectrometry: Morphology Selective Binding of Fabs to Hepatitis B Virus Capsids, *Anal. Bioanal. Chem.*, 2014, **406**, 1437–1446.
10 C. Uetrecht, C. Versluis, N. R. Watts, W. H. Roos, G. J. L. Wuite, P. T. Wingfield, A. C. Steven and A. J. R. Heck, High-Resolution Mass Spectrometry of Viral Assemblies: Molecular Composition and Stability of Dimorphic Hepatitis B Virus Capsids, *Proc. Natl. Acad. Sci. U. S. A.*, 2008, **105**, 9216–9220.
11 D. Z. Keifer, A. W. Alexander and M. F. Jarrold, Spontaneous Mass and Charge Losses From Single Multi-Megadalton Ions Studied by Charge Detection Mass Spectrometry, *J. Am. Soc. Mass Spectrom.*, 2017, **28**, 498–506.
12 N. Tahallah, M. Pinkse, C. S. Maier and A. J. R. Heck, The Effect of the Source Pressure on the Abundance of Ions of Noncovalent Protein Assemblies in an Electrospray Ionization Orthogonal Time-of-Flight Instrument, *Rapid Commun. Mass Spectrom.*, 2001, **15**, 596–601.
13 A. N. Krutchinsky, A. V. Loboda, V. L. Spicer, R. Dworschak, W. Ens and K. G. Standing, Orthogonal Injection of Matrix-Assisted Laser Desorption/Ionization Ions into a Time-of-Flight Spectrometer through a Collisional Damping Interface, *Rapid Commun. Mass Spectrom.*, 1998, **12**, 508–518.
14 I. V. Chernushevich and B. A. Thomson, Collisional Cooling of Large Ions in Electrospray Mass Spectrometry, *Anal. Chem.*, 2004, **76**, 1754–1760.
15 K. Lorenzen, C. Versluis, E. van Duijn, R. H. H. van den Heuvel and A. J. R. Heck, Optimizing Marcomolecular Tandem Mass Spectrometry of Large Non-Covalent Complexes Using Heavy Collision Gases, *Int. J. Mass Spectrom.*, 2007, **268**, 198–206.
16 S. K. Chowdhury, V. Katta and B. T. Chait, An Electrospray-Ionization Mass Spectrometer with New Features, *Rapid Commun. Mass Spectrom.*, 1990, **4**, 81–87.
17 M. A. Tito, K. Tars, K. Valegard, J. Hajdu and C. V. Robinson, Electrospray Time-of-Flight Mass Spectrometry of the Intact MS2 Virus Capsid, *J. Am. Chem. Soc.*, 2000, **122**, 3550–3551.
18 J. Snijder, M. van de Waterbeemd, E. Damoc, E. Denisov, D. Grinfeld, A. Bennett, M. Agbandje-mcKenna, A. Makarov and A. J. R. Heck, Defining the Stoichiometry and Cargo Load of Viral and Bacterial Nanoparticles by Orbitrap Mass Spectrometry, *J. Am. Chem. Soc.*, 2014, **136**, 7295–7299.
19 R. Antoine, T. Doussineau, P. Dugourd and F. Calvo, Multiphoton Dissociation of Macromolecular Ions at the Single-Molecule Level, *Phys. Rev. A*, 2013, **87**, 013435.
20 T. Doussineau, P. Paletto, P. Dugourd and R. Antoine, Multiphoton Dissociation of Electrosprayed MegaDalton-Sized DNA Ions in a Charge-Detection Mass Spectrometer, *J. Am. Soc. Mass Spectrom.*, 2015, **26**, 7–13.
21 D. Z. Keifer and M. F. Jarrold, Single-Molecule Mass Spectrometry, *Mass Spectrom. Rev.*, 2017, DOI: 10.1002/mas.21495.
22 R. D. Smith, X. Cheng, J. E. Bruce, S. A. Hofstadler and G. A. Anderson, Trapping, Detection and Reaction of Very Large Single Molecular Ions by Mass Spectrometry, *Nature*, 1994, **369**, 137–139.
23 J. E. Bruce, X. Cheng, R. Bakhtiar, Q. Wu, S. A. Hofstadler, G. A. Anderson and R. D. Smith, Trapping, Detection, and Mass Measurement of Individual Ions in a Fourier Transform Ion Cyclotron Resonance Mass Spectrometer, *J. Am. Chem. Soc.*, 1994, **116**, 7839–7847.
24 M. A. Philip, F. Gelbard and S. Arnold, An Absolute Method for Aerosol Particle Mass and Charge Measurement, *J. Colloid Interface Sci.*, 1983, **91**, 507–515.
25 G. Hars and Z. Tass, Application of Quadrupole Ion Trap for the Accurate Mass Determination of Submicron Size Charged Particles, *J. Appl. Phys.*, 1995, **77**, 4245–4250.
26 S. Schlemmer, J. Illemann, S. Wellert and D. Gerlich, Nondestructive High-Resolution and Absolute Mass Determination of Single Charged Particles in a Three-Dimensional Quadrupole Trap, *J. Appl. Phys.*, 2001, **90**, 5410–5418.
27 C. R. Howder, B. A. Long, D. M. Bell, K. H. Furakawa, R. C. Johnson, Z. Fang and S. L. Anderson, Photoluminescence of Charged CdSe/ZnS Quantum Dots in the Gas Phase: Effects of Charge and Heating on Absorption and Emission Probabilities, *ACS Nano*, 2014, **8**, 12534–12548.
28 S. Dohn, W. Svendsen and A. Boisen, Mass and Position Determination of Attached Particles on Cantilever Based Mass Sensors, *Rev. Sci. Instrum.*, 2007, **78**, 103303.
29 M. S. Hanay, S. Kelber, A. K. Naik, D. Chi, S. Hentz, E. C. Bullard, E. Colinet, L. Duraffourg and M. L. Roukes, Single-Protein Nanomechanical Mass Spectrometry in Real time, *Nat. Nanotechnol.*, 2012, **7**, 602–608.
30 E. Sage, A. Brenac, T. Alava, R. Morel, C. Dupré, M. S. Hanay, M. L. Roukes, L. Duraffourg, C. Masselon and S. Hentz, Neutral Particle Mass Spectrometry with Nanomechanical Systems, *Nat. Commun.*, 2015, **6**, 6482.
31 R. Chen, Q. Wu, D. W. Mitchell, S. A. Hofstadler, A. L. Rockwood and R. D. Smith, Direct Charge Number and Molecular Weight Determination of Large Individual Ions by Electrospray Ionization Fourier Transform Ion

 

Cyclotron Resonance Mass Spectrometry, *Anal. Chem.*, 1994, **66**, 3964–3969.

32 W.-P. Peng, H.-C. Lin, H.-H. Lin, M. Chu, A. L. Yu, H.-C. Chang and H.-C. Chen, Charge-Monitoring Laser-Induced Acoustic Desorption Mass Spectrometry for Cell and Microparticle Mass Distribution Measurement, *Angew. Chem., Int. Ed.*, 2007, **46**, 3865–3869.

33 Z. Nie, F. Cui, M. Chu, C.-H. Chen, H.-C. Chang and Y. Cai, Calibration of a Frequency-Scan Quadrupole Ion Trap Mass Spectrometer for Microparticle Mass Analysis, *Int. J. Mass Spectrom.*, 2008, **270**, 8–15.

34 M. Frank, S. E. Labov, G. Westmacott and W. H. Benner, Energy-Sensitive Cryogenic Detectors for High-Mass Biomolecule Mass Spectrometry, *Mass Spectrom. Rev.*, 1999, **18**, 155–186.

35 M. W. Rabin, G. C. Hilton and J. M. Martinis, Application of Microcalorimeter Energy Measurement to Biopolymer Mass Spectrometry, *IEEE Trans. Appl. Supercond.*, 2001, **11**, 242–247.

36 R. J. Wenzel, U. Matter, L. Schultheis and R. Zenobi, Analysis of Megadalton Ions Using Cryodetection MALDI Time-of-Flight Mass Spectrometry, *Anal. Chem.*, 2005, **77**, 4329–4337.

37 W. Shockley, Currents to Conductors Induced by a Moving Point Charge, *J. Appl. Phys.*, 1938, **9**, 635–636.

38 A. J. Weinheimer, The Charge Induced on a Conducting Cylinder by a Point Charge and Its Application to the Measurement of Charge on Precipitation, *J. Atmos. Oceanic Technol.*, 1988, **5**, 298–304.

39 H. Shelton, C. D. Hendricks and R. F. Wuerker, Electrostatic Acceleration of Microparticles to Hypervelocities, *J. Appl. Phys.*, 1960, **31**, 1243–1246.

40 J. F. Friichtenicht, Micrometeoroid Simulation Using Nuclear Accelerator Techniques, *Nucl. Instrum. Methods*, 1964, **28**, 70–78.

41 V. Rudolph, Massen-Geschwindigkeitsfilter für Künstlich Beschleunigten Staub, *Z. Naturforsch. Ser. A*, 1966, **21**, 1993–1996.

42 G. L. Stradling, G. C. Idzorek, B. P. Shafer, H. L. Curling Jr., M. T. Collopy, A. A. Hopkins Blossom and S. Fuerstenau, Ultra-High Velocity Impacts: Cratering Studies of Microscopic Impacts from 3 km/s to 30 km/s, *Int. J. Impact Eng.*, 1993, **14**, 719–727.

43 B. D. Adamson, M. E. C. Miller and R. E. Continetti, The Aerosol Impact Spectrometer: A Versatile Platform for Studying the Velocity Dependence of Nanoparticle-Surface Impact Phenomena, *EPJ TI*, 2017, in press, DOI:DOI: 10.1140/epjti/s40485-017-0037-6.

44 S. D. Fuerstenau and W. H. Benner, Molecular Weight Determination of Megadalton DNA Electrospray Ions Using Charge Detection Time-of-Flight Mass Spectrometry, *Rapid Commun. Mass Spectrom.*, 1995, **9**, 1528–1538.

45 J. C. Schultz, C. A. Hack and W. H. Benner, Mass Determination of Megadalton-DNA Electrospray Ions Using Charge Detection Mass Spectrometry, *J. Am. Soc. Mass Spectrom.*, 1998, **9**, 305–313.

46 J. C. Schultz, C. A. Hack and W. H. Benner, Polymerase Chain Reaction Products Analyzed by Charge Detection Mass Spectrometry, *Rapid Commun. Mass Spectrom.*, 1999, **13**, 15–20.

47 S. D. Fuerstenau, W. H. Benner, J. J. Thomas, C. Brugidou, B. Bothner and G. Siuzdak, Mass Spectrometry of an Intact Virus, *Angew. Chem., Int. Ed.*, 2001, **113**, 559–562.

48 T. Doussineau, M. Kerleroux, X. Dagany, C. Clavier, M. Barbaire, J. Maurelli, R. Antoine and P. Dugourd, Charging Megadalton Poly(Ethylene Oxide)s by Electrospray Ionization. A Charge Detection Mass Spectrometry Study, *Rapid Commun. Mass spectrum.*, 2011, **25**, 617–623.

49 T. Doussineau, C. Y. Bao, R. Antoine, P. Dugourd, W. Zhang, F. D'Agosto and B. Charleux, Direct Molar Mass Determination of Self-Assembled Amphiphilic Block Copolymer Nanoobjects Using Electrospray-Charge Detection Mass Spectrometry, *ACS Macro Lett.*, 2012, **1**, 414–417.

50 T. Doussineau, M. Santacreu, R. Antoine, P. Dugourd, W. Zhang, I. Chaduc, M. Lansalot, F. D'Agosto and B. Charleux, The Charging of Micellar Nanoparticles in Electrospray Ionization, *ChemPhysChem*, 2013, **14**, 603–609.

51 T. Doussineau, A. Désert, O. Lambert, J.-C. Taveau, M. Lansalot, P. Dugourd, E. Bourgeat-lami, S. Ravaine, E. Duguet and R. Antoine, Charge Detection Mass Spectrometry for the Characterization of Mass and Surface Area of Composite Nanoparticles, *J. Phys. Chem. C*, 2015, **119**, 10844–10849.

52 N. Ouadah, T. Doussineau, T. Hamada, P. Dugourd, C. Bordes and R. Antoine, Correlation between the Charge of Polymer Particles in Solution and in the Gas Phase Investigated by Zeta-Potential Measurements and Electrospray Ionization Mass Spectrometry, *Langmuir*, 2013, **29**, 14074–14081.

53 N. J. Warren, O. O. Mykhaylyk, A. J. Ryan, M. Williams, T. Doussineau, P. Dugourd, R. Antoine, G. Portale and S. P. Armes, Testing the Vesicular Morphology to Destruction: Birth and Death of Diblock Copolymer Vesicles Prepared via Polymerization-Induced Self-Assembly, *J. Am. Chem. Soc.*, 2015, **137**, 1929–1937.

54 J. T. Maze, T. C. Jones and M. F. Jarrold, Negative Droplets from Positive Electrospray, *J. Phys. Chem. A*, 2006, **110**, 12607–12612.

55 S. R. Mabbett, L. W. Zilch, J. T. Maze, J. W. Smith and M. F. Jarrold, Pulsed Acceleration Charge Detection Mass Spectometry: Application to Weighing Electrosprayed Droplets, *Anal. Chem.*, 2007, **79**, 8431–8439.

56 L. W. Zilch, J. T. Maze, J. W. Smith, G. E. Ewing and M. F. Jarrold, Charge Separation in the Aerodynamic Breakup of Micrometer-Sized Water Droplets, *J. Phys. Chem. A*, 2008, **112**, 13352–13363.

57 A. Viodé, X. Dagany, M. Kerleroux, P. Dugourd, T. Doussineau, L. Charles and R. Antoine, Coupling of Size-Exclusion Chromatography with Electrospray Ionization Charge-Detection Mass Spectrometry for the

Characterization of Synthetic Polymers of Ultra-High Molar Mass, *Rapid Commun. Mass Spectrom.*, 2016, **30**, 132–136.
58 J. W. Smith, E. E. Siegel, J. T. Maze and M. F. Jarrold, Image Charge Detection Mass Spectrometry: Pushing the Envelope with Sensitivity and Accuracy, *Anal. Chem.*, 2011, **83**, 950–956.
59 M. Gamero-castaño, Induction Charge Detector with Multiple Sensing Stages, *Rev. Sci. Instrum.*, 2007, **78**, 043301.
60 M. Gamero-castaño, Retarding Potential and Induction Charge Detectors in Tandem for Measuring the Charge and Mass of Nanodroplets, *Rev. Sci. Instrum.*, 2009, **80**, 053301.
61 B. L. Barney, R. T. Daly and D. E. Austin, A Multi-Stage Image Charge Detector Made from Printed Circuit Boards, *Rev. Sci. Instrum.*, 2013, **84**, 114101.
62 W. H. Benner, A Gated Electrostatic Ion Trap to Repetitiously Measure the Charge and *m*/*z* of Large Electrospray Ions, *Anal. Chem.*, 1997, **69**, 4162–4168.
63 T. Doussineau, C. Y. Bao, C. Clavier, X. Dagany, M. Kerleroux, R. Antoine and P. Dugourd, Infrared Multiphoton Dissociation Tandem Charge Detection-Mass Spectrometry of Single Megadalton Electrosprayed Ions, *Rev. Sci. Instrum.*, 2011, **82**, 084104.
64 H. T. Schmidt, H. Cederquist, J. Jensen and A. Fardi, Conetrap: A Compact Electrostatic Ion Trap, *Nucl. Instrum. Methods Phys. Res., Sect. B*, 2001, **173**, 523–527.
65 N. C. Contino and M. F. Jarrold, Charge Detection Mass Spectrometry for Single Ions with a Limit of Detection of 30 Charges, *Int. J. Mass Spectrom.*, 2013, **345–347**, 153–159.
66 E. E. Pierson, N. C. Contino, D. Z. Keifer and M. F. Jarrold, Charge Detection Mass Spectrometry for Single Ions with an Uncertainty in the Charge Measurement of 0.65 e, *J. Am. Soc. Mass Spectrom.*, 2015, **26**, 1213–1220.
67 N. C. Contino, E. E. Pierson, D. Z. Keifer and M. F. Jarrold, Charge Detection Mass Spectrometry with Resolved Charge States, *J. Am. Soc. Mass Spectrom.*, 2013, **24**, 101–108.
68 D. Z. Keifer, D. L. Shinholt and M. F. Jarrold, Charge Detection Mass Spectrometry with Almost Perfect Charge Accuracy, *Anal. Chem.*, 2015, **87**, 10330–10337.
69 A. G. Elliot, S. I. Merenbloom, S. Chakrabarty and E. R. Williams, Single Particle Analyzer of Mass: A Charge Detection Mass Spectrometer With a Multi-Detector Electrostatic Ion Trap, *Int. J. Mass Spectrom.*, 2017, **414**, 45–55.
70 B. L. Karger and A. Guttman, DNA Sequencing by Capillary Electrophoresis, *Electrophoresis*, 2009, **1**, S196–S202.
71 T. Doussineau, R. Antoine, M. Santacreu and P. Dugourd, Pushing the Limit of Infrared Multiphoton Dissociation to Megadalton-Size DNA Ions, *J. Phys. Chem. Lett.*, 2012, **3**, 2141–2145.
72 H. Hernandez and C. V. Robinson, Determining the Stoichiometry and Interactions of Macromolecular Assemblies from Mass Spectrometry, *Nat. Protoc.*, 2007, **2**, 715–726.
73 E. E. Pierson, D. Z. Keifer, N. C. Contino and M. F. Jarrold, Probing Higher Order Multimers of Pyruvate Kinase with Charge Detection Mass Spectrometry, *Int. J. Mass Spectrom.*, 2013, **337**, 50–56.
74 T. Doussineau, C. Mathevon, L. Altamura, C. Vendrely, P. Dugourde, V. Forge and R. Antoine, Mass Determination of Entire Amyloid Fibrils by Using Mass Spectrometry, *Angew. Chem., Int. Ed.*, 2016, **128**, 2386–2390.
75 C. Bleiholder, N. F. Dupuis, T. Wyttenbach and M. T. Bowers, Ion Mobility-Mass Spectrometry Reveals a Conformational Conversion from Random Assembly to β-Sheet in Amyloid Fibril Formation, *Nat. Chem.*, 2010, **3**, 172–177.
76 G. Siuzdak, B. Bothner, M. Yeager, C. Brugidou, C. M. Fauquet, K. Hoey and C.-M. Chang, Mass Spectrometry and Viral Analysis, *Chem. Biol.*, 1996, **3**, 45–48.
77 B. Bothner and G. Siuzdak, Electrospray Ionization of a Whole Virus: Analyzing Mass, Structure, and Viability, *ChemBioChem*, 2004, **5**, 258–260.
78 D. L. D. Caspar and A. Klug, Physical Principles in the Construction of Regular Viruses, *Cold Spring Harbor Symp. Quant. Biol.*, 1962, **27**, 1–24.
79 A. Zlotnick, To Build a Virus Capsid, *J. Mol. Biol.*, 1994, **241**, 59–67.
80 C. Uetrecht, I. M. Barbu, G. K. Shoemaker, E. van Duijn and A. J. Heck, Interrogating Viral Capsid Assembly With Ion Mobility-Mass Spectrometry, *Nat. Chem.*, 2011, **3**, 126–132.
81 E. E. Pierson, D. Z. Keifer, L. S. Lee, N. C. Contino, J. C.-Y. Wang, A. Zlotnick and M. F. Jarrold, Detection of Late Intermediates in Virus Capsid Assembly by Charge Detection Mass Spectrometry, *J. Am. Chem. Soc.*, 2014, **136**, 3536–3541.
82 C. Chen, J. C.-Y. Wang, E. E. Pierson, D. Z. Keifer, M. Delaleau, L. Gallucci, C. Cazenave, M. Kann, M. F. Jarrold and A. Z. Lotnick, Importin β Can Bind Hepatitis B Virus Core Protein and Empty Core-Like Particles and Induce Structural Changes, *PLoS Pathog.*, 2016, **12**, e1005802.
83 A. A. Kukreja, J. C.-Y. Wang, E. E. Pierson, D. Z. Keifer, L. Selzer, Z. Tan, B. Dragnea, M. F. Jarrold and A. Zlotnick, Structurally Similar Woodchuck and Human Hepadnavirus Core Proteins Have Distinctly Different Temperature Dependences of Assembly, *J. Virol.*, 2014, **88**, 14105–14115.
84 E. E. Pierson, D. Z. Keifer, A. A. Kukreja, J. C.-Y. Wang, A. Zlotnick and M. F. Jarrold, Charge Detection Mass Spectrometry Identifies Preferred Non-Icosahedral Polymorphs in the Self-Assembly of Woodhuck Hepatitis Virus Capsids, *J. Mol. Biol.*, 2016, **428**, 292–300.
85 A. Luque and D. Reguera, The Structure of Elongated Viral Capsids, *Biophys. J.*, 2010, **98**, 2993–3003.
86 E. E. Pierson, D. Z. Keifer, A. Asokan and M. F. Jarrold, Resolving Adeno-Associated Viral Particle Diversity With Charge Detection Mass Spectrometr, *Anal. Chem.*, 2016, **88**, 6718–6725.

 

87 D. Z. Keifer, E. E. Pierson, J. A. Hogan, G. J. Bedwell, P. E. Pregelige and M. F. Jarrold, Charge Detection Mass Spectrometry of Bacteriophage P22 Procapsid Distributions Above 20 MDa, *Rapid Commun. Mass Spectrom.*, 2014, **28**, 483–488.

88 M. M. Suhanovsky and C. M. Teschke, Bacteriophage P22 Capsid Size Determination: Roles for the Coat Protein Telokin-Like Domain and the Scaffolding Protein Amino-Terminus, *Virology*, 2011, **417**, 418–429.

89 D. Z. Keifer, T. Motwani, C. M. Teschke and M. F. Jarrold, Acquiring Structural Information on Virus Particles with Charge Detection Mass Spectrometry, *J. Am. Soc. Mass Spectrom.*, 2016, **6**, 1028–1036.

90 L. Rayleigh, On the Equilibrium of Liquid Conducting Masses Charged With Electricity, *Philos. Mag., Ser. 5*, 1882, **14**, 184–186.

91 J. Fernandez de la Mora, Electrospray Ionization of Large Multiply Charged Species Proceeds Via Dole's Charged Residue Mechanism, *Anal. Chim. Acta*, 2000, **406**, 93–104.

92 A. J. R. Heck and R. H. H. Van den Heuvel, Investigation of Intact Protein Complexes by Mass Spectrometry, *Mass Spectrom. Rev.*, 2004, **23**, 368–389.

93 D. Z. Keifer, T. Motwani, C. M. Teschke and M. F. Jarrold, Measurement of the Accurate Mass of a 50 MDa Infectious Virus, *Rapid Commun. Mass Spectrom.*, 2016, **30**, 1957–1962.